

Controls on the spacing and geometry of rill networks on hillslopes: Rain splash detachment, initial hillslope roughness, and the competition between fluvial and colluvial transport

Luke A. McGuire,¹ Jon D. Pelletier,^{1,2} José A. Gómez,³ and Mark A. Nearing⁴

Received 29 June 2012; revised 20 December 2012; accepted 21 December 2012; published 20 March 2013.

[1] Rill networks have been a focus of study for many decades, but we still lack a complete understanding of the variables that control the spacing of rills and the geometry of rill networks (e.g., parallel or dendritic) on hillslopes. In this paper, we investigate the controls on the spacing and geometry of rill networks using numerical modeling and comparison of the model results to terrestrial-laser-scanner-derived topographic data from rill networks formed in physical experiments. The landscape evolution model accounts for the transport of sediment due to rain splash and fluvial entrainment as well as the deposition of sediment being advected by the overland flow. In order to develop realistic rill networks in the model, we find that it is necessary to incorporate the effects of raindrop impact within the fluvial sediment transport process. Model results are only consistent with those of experiments when raindrop-aided fluvial sediment transport is accounted for. Dendritic networks are often predicted by the model in cases of high initial topographic roughness and high rates of advective (fluvial) sediment transport relative to diffusive (colluvial) transport. Parallel networks form within numerical experiments in low-roughness cases under a wide range of relative advective and diffusive transport rates as well as in high roughness cases in which diffusive sediment transport is high relative to advective transport. The transition from dendritic to parallel rill networks is shown to occur gradually rather than being associated with a particular threshold. Finally, based on a balance between diffusive and advective sediment transport processes, we predict that the mean spacing between parallel rills scales with the square root of the ratio of diffusivity to channel erodibility.

Citation: McGuire, L. A., J. D. Pelletier, J. A. Gómez, and M. A. Nearing (2013), Controls on the spacing and geometry of rill networks on hillslopes: Rain splash detachment, initial hillslope roughness, and the competition between fluvial and colluvial transport, *J. Geophys. Res. Earth Surf.*, 118, 241–256, doi:10.1002/jgrf.20028.

1. Introduction

[2] Feedback mechanisms between overland flow and sediment transport can lead to the development of drainage patterns with remarkably uniform patterns [Perron *et al.*, 2008]. At the hillslope scale, the study of rills has attracted considerable attention due to their pattern-forming nature [Favis-Mortlock *et al.*, 2000] and their ability to enhance sediment transport rates relative to un-dissected hillslopes. Rills

are small, erosional incisions (0.01–0.1 m) within the soil, commonly found on steep hillslopes with little or no vegetation. The large number of possible sediment transport mechanisms on hillslopes and their tendency to vary significantly in relative magnitude with environmental factors have made it difficult to determine the controlling factors of rill network geometry. A better understanding of the controls on rill network geometry would improve our ability to more accurately model and predict erosion at the hillslope scale. In particular, relationships between surface roughness, mean slope, and rill development can serve to improve parameterizations of rilling within larger-scale landscape evolution models that are not capable of resolving features at such scales (i.e., 0.01–1 m).

[3] Previous studies [e.g., Smith and Bretherton, 1972; Loewenherz, 1991; Simpson and Schlunegger, 2003; Simpson and Castellort, 2006; Smith, 2010] have developed mathematical models that account for the interaction between overland flow and sediment transport that lead to channel networks. Simpson and Schlunegger [2003], for example, demonstrated that the geometries of channel networks formed on initially un-dissected landscapes are influenced by the

¹Program in Applied Mathematics, University of Arizona, Tucson, Arizona, USA.

²Department of Geosciences, University of Arizona, Tucson, Arizona, USA.

³Instituto de Agricultura Sostenible, Cordoba, Spain.

⁴United States Department of Agriculture, Agricultural Research Service, Tucson, Arizona, USA.

Corresponding author: L. A. McGuire, Program in Applied Mathematics, University of Arizona, 617 N. Santa Rita Ave., Tucson, AZ 85721, USA. (lmcguire@math.arizona.edu)

relative importance of fluvial sediment transport and colluvial transport. The feedbacks between topography and overland flow can lead to the development of valley networks, while colluvial sediment transport, which has a diffusive effect on the land surface, can act to smooth the landscape. Significant work has also been done using physical models to study the evolution of rill networks on different initial surfaces [e.g., Gomez *et al.*, 2003; Rieke-Zapp and Nearing, 2005] and to establish the conditions for rill initiation [e.g., Gilley *et al.*, 1993; Yao *et al.*, 2008]. Despite our ability to produce, model, and observe the processes of rill initiation and development, it remains difficult to adequately identify and quantitatively describe the controls on different rill network geometries.

[4] Because of the coupling among topography, water flow, and erosion/deposition, it is likely that any channel system will depend on the initial surface roughness because roughness sets the initial overland flow pathways. Micro-topographic roughness contributes to the concentration of overland flow, which in turn leads to the initial success of some incipient channels over others. The subsequent development of the network also depends on the relative importance of different sediment transport mechanisms. Studies of large-scale channel systems (i.e., incised-valley drainage networks rather than rill networks) often focus on either sediment transport mechanisms or initial topographic roughness as the dominant controls on drainage network development. Perron *et al.* [2008], for example, demonstrated the importance of a landscape Peclet number, which quantifies the relative importance of advective and diffusive sediment transport processes, in their study of the controls on the periodic spacing of first-order valleys. Relationships have also been suggested between the structure of river networks and regional slope [Castelltort *et al.*, 2009; Jung *et al.*, 2011]. Such studies suggest a threshold value for the regional slope above which parallel networks tend to occur more often than dendritic networks. On smaller scales, there is strong evidence that micro-topography influences rill network geometry by preferentially routing runoff and localizing erosion in a positive feedback [Favis-Mortlock, 1998; Favis-Mortlock *et al.*, 2000]. Simpson and Schlunegger [2003] used a numerical model to show that parallel networks tend to develop in cases where the relative magnitude of initial roughness is small and that increases in roughness can lead to more dendritic patterns. These authors also considered the relative importance of two different sediment transport mechanisms, namely, fluvial and colluvial transport, on channel formation and described a process in which the final channel network geometry is dependent upon the timescale at which diffusive smoothing removes roughness elements from the initial surface. They suggested that rill-like features commonly form on smaller spatial scales due to the fact that mean slope tends to dominate surface roughness on the hillslope scale, whereas this is not as often the case on the scale at which river networks form [Simpson and Schlunegger, 2003]. We build upon previous studies by (1) demonstrating the importance of raindrop-aided sediment transport in hillslope-scale erosion problems, (2) demonstrating the existence of a smooth transition from parallel to dendritic rill networks, and (3) developing a scaling relationship to predict mean rill spacing within parallel networks.

[5] Given that parameterizations of rates of sediment transport and erosion/deposition are highly empirical and often the most poorly constrained aspect of this and similar landscape evolution models, it is essential to test the predictions of

hillslope-scale landscape evolution models against data from physical experiments whenever possible. Gomez *et al.* [2003] performed a series of physical experiments where rill networks were formed over a 5 h period of generated rainfall on a 2 m by 4 m flume inclined at either a 20% or 5% slope. Experiments were carried out on three different types of surfaces characterized by varying degrees of surface roughness: low, medium, and high. Gomez *et al.* [2003] performed two replications for each slope and surface treatment. Terrestrial-laser-scanner-derived digital elevation models (DEM) were created for the initial surface as well as the surface after each hour of simulated rainfall. Experimental data corresponding to the two replications performed on the 20% slope with low surface roughness are chosen for comparison with the numerical model, as they give rise to the most well developed and clearly defined rill networks.

2. Conceptual Model

[6] The landscape evolution equation we employ is designed to represent three processes: the direct transport of material due to rain splash, the fluvial detachment and transport of bed material disturbed by raindrop impact, and the deposition of sediment being advected within overland flow. The impact of raindrops is directly responsible for transporting bed material through rain splash. Rain splash is generally represented as a transport-limited process in which the sediment flux is proportional to the land-surface gradient [Dunne *et al.*, 2010]. Raindrop impact can also indirectly influence rates of fluvial transport by detaching and disaggregating soil particles and making them more transportable by overland flow [Nord and Esteves, 2005]. Experiments have documented order of magnitude differences in sediment concentrations when overland flow within small plots of cohesive soil is induced by rainfall as opposed to flow from a ground level perforated pipe, suggesting that overland flow may be ineffective at detaching sediment without raindrop impact [Gabet and Dunne, 2003].

[7] Previous studies have introduced models that account for differences between unaltered, in situ soil, and an overlying sediment layer that can develop through a combination of rain splash detachment and re-deposition [e.g., Hairsine and Rose, 1991, 1992a, 1992b; Heng *et al.*, 2011]. Hairsine and Rose [1992a] presented an erosion model that explicitly accounts for the entrainment and re-entrainment of sediment into the overland flow column due to raindrop impact, entrainment and re-entrainment due to overland flow, deposition of sediment, and the difference in erodibility between a re-deposited layer of sediment and the original (usually more cohesive) bed material. Nord and Esteves [2005] modeled erosion as occurring in multiple phases. During the first phase, the flow has not yet overcome critical thresholds necessary to transport material, and the breakdown of aggregates, raindrop impact, rain splash, and the resulting deposition contribute to the formation of a layer of loose sediment. The land-surface elevation does not change during this initial phase. This sediment is then available for fluvial transport once an entrainment threshold is reached. Once the layer of loose sediment is removed, the flow is capable of detaching unaltered bed material if a second, more stringent threshold is achieved. The transport of unaltered soil, which is less erodible, is considered to be negligible in this study.

[8] The model presented in this study accounts for many of the same sediment transport mechanisms as the model suggested by *Hairsine and Rose* [1991, 1992a, 1992b]. Both models allow for the development of a layer of sediment overlying the in situ soil, although here it is possible for this overlying layer to form without the deposition of previously entrained sediment. Here raindrop impact converts the soil into a more easily detachable (damaged) layer of material at a rate dependent on overland flow depth. The rate depends on overland flow depth because overland flows that are sufficiently deep absorb momentum from the raindrops and protect the underlying soil from impact [Dunne *et al.*, 2010]. The deposition of previously entrained material is thought to add directly to the damaged layer of sediment. Sediment within the damaged layer is capable of being detached and transported by the flow at any time, given that such material exists and any critical entrainment thresholds are exceeded. In this way, raindrop impact acts as a limiting factor for the rate of fluvial detachment of sediment. The direct transport of sediment through rain splash is accounted for independently from fluvial transport. The interaction between shallow overland flow, raindrop impact, and soil

is a complex process dependent upon both raindrop size and velocity as well as overland flow depth [Kinnell, 1991]. The model introduced here is a simple way to account for the fact that fluvial sediment transport may still take place, but in a manner limited by the ability of raindrop impact to affect the soil, even when overland flow itself is insufficient to entrain and transport unaltered bed material. This is a reasonable assumption for the hillslope scale, but on a larger scale, it is likely that valley-like features will begin to form once the typical stream power (or shear stress) becomes sufficiently large to exceed the critical value necessary to entrain unaltered soil.

3. Methods

3.1. Governing Equations

[9] A rainfall rate, R , in excess of infiltration results in overland flow with depth h , an x component of velocity u , and a y component of velocity v . The model equations used to govern quasi-steady flow are given by [Simpson and Castellort, 2006]

$$\frac{\partial(hu)}{\partial x} + \frac{\partial(hv)}{\partial y} = R + \frac{E - D}{1 - \phi} \quad (1)$$

$$\frac{\partial}{\partial x} \left(hu^2 + \frac{1}{2}gh^2 \right) + \frac{\partial}{\partial y} (huv) = \gamma_x \quad (2)$$

$$\frac{\partial}{\partial x} (huv) + \frac{\partial}{\partial y} \left(hv^2 + \frac{1}{2}gh^2 \right) = \gamma_y \quad (3)$$

$$\frac{\partial(hcu)}{\partial x} + \frac{\partial(hcv)}{\partial y} = E - D \quad (4)$$

[10] Equations (1)–(3) represent conservation of water, conservation of momentum in the x direction, and conservation of momentum in the y direction, respectively. The fourth equation enforces the conservation of sediment with c denoting sediment concentration. Bed sediment porosity and gravitational acceleration are denoted by ϕ and g , respectively (see Table 1 for notation). The forcing terms in the momentum equations are defined as

$$\gamma_x = -gh \frac{\partial z}{\partial x} - \frac{fv\sqrt{u^2 + v^2}}{8} + \epsilon \left(\frac{\partial^2 hu}{\partial x^2} + \frac{\partial^2 hu}{\partial y^2} \right) - \frac{(\rho_s - \rho_w)gh^2}{2\rho} \frac{\partial c}{\partial x} - \frac{(\rho_0 - \rho)(E - D)u}{\rho(1 - \phi)} \quad (5)$$

and

$$\gamma_y = -gh \frac{\partial z}{\partial y} - \frac{fv\sqrt{u^2 + v^2}}{8} + \epsilon \left(\frac{\partial^2 hv}{\partial x^2} + \frac{\partial^2 hv}{\partial y^2} \right) - \frac{(\rho_s - \rho_w)gh^2}{2\rho} \frac{\partial c}{\partial y} - \frac{(\rho_0 - \rho)(E - D)v}{\rho(1 - \phi)}. \quad (6)$$

[11] Here f denotes the Darcy-Weisbach friction factor and $\epsilon \approx 10^{-4}$ is the coefficient of turbulent viscosity. From left to right, the forcing terms account for the effects of topography, friction, turbulent dissipation, a spatially variable sediment concentration, and momentum transfer associated with sediment exchange between the flow and the bed. The density of the sediment and water are defined as $\rho_s = 2600 \text{ kg m}^{-3}$ and

Table 1. Notation

Symbol	Unit	Definition
z	m	Topographic elevation
h	m	Water depth
uh	$\text{m}^2 \text{ s}^{-1}$	Unit fluid discharge (x direction)
vh	$\text{m}^2 \text{ s}^{-1}$	Unit fluid discharge (y direction)
u	m s^{-1}	Fluid velocity (x direction)
v	m s^{-1}	Fluid velocity (y direction)
g	m s^{-2}	Gravitational acceleration
c	–	Sediment concentration
f	–	Darcy-Weisbach friction factor
ϵ	$\text{m}^2 \text{ s}^{-1}$	Coefficient of turbulent viscosity
h_c	m	Critical overland flow depth
ζ	m s^{-1}	Maximum soil damage rate
v	m	Depth of damaged sediment layer
d	m	Particle diameter
v_s	cm s^{-1}	Particle settling velocity
R	m s^{-1}	Rainfall rate in excess of infiltration
κ	m^{-1}	Stream power erodibility coefficient
κ_s	$\text{m}^2 \text{ s kg}^{-1}$	Shear stress erodibility coefficient
β	$\text{m}^2 \text{ s}^{-1}$	Diffusivity
τ	Pa	Shear stress
τ_c	Pa	Critical shear stress
Ω	$\text{m}^2 \text{ s}^{-1}$	Unit stream power
Ω_c	$\text{m}^2 \text{ s}^{-1}$	Critical unit stream power
E	m s^{-1}	Sediment entrainment rate
D	m s^{-1}	Sediment deposition rate
r_d	mm	Raindrop diameter
v_t	m s^{-1}	Particle takeoff velocity
α_0	deg.	Particle takeoff angle
θ_s	deg.	Bed slope
ϕ	–	Bed sediment porosity
ρ_w	kg m^{-3}	Density of water
ρ_s	kg m^{-3}	Density of sediment
ρ	kg m^{-3}	Density of sediment-water mixture
ρ_0	kg m^{-3}	Density of saturated bed
η	m	Variance of initial surface roughness
δ	m	Spacing of roughness elements
L_0	m	Characteristic slope length (along-slope direction)
R_0	m s^{-1}	Characteristic rainfall rate
κ'	s^{-1}	Inverse of advection timescale ($=\kappa R_0$)
β'	s^{-1}	Inverse of diffusion timescale ($=\beta/L_0^2$)
θ	–	Landscape Peclet number ($=\beta'/\kappa'$)
λ	m	Length scale of parallel rill spacing
J_r	–	Number of rill junctions/number of rills

$\rho_w = 1000 \text{ kg m}^{-3}$, respectively, while $\rho_0 = \rho_w \phi + \rho_s(1 - \phi)$ is the density of the saturated bed and $\rho = \rho_w(1 - c) + \rho_s c$ is the density of the sediment-water mixture. An additional term of the form $Rcu(\rho_s - \rho_w)/\rho$ is sometimes included within γ_x (and a similar term within γ_y) [Li and Duffly, 2011] but is neglected here. Within rill flow, one can estimate $c \approx 0.01$, $u \approx 0.1$, and $R \approx 10^{-5}$, which implies $Rcu(\rho_s - \rho_w)/\rho \sim 10^{-8}$ with smaller values being expected in inter-rill locations. The smallest term included within the momentum equation is the term associated with turbulent viscosity, which scales with $cuh \sim 10^{-7}$ when assuming a length scale on the order of unity, $u \approx 0.1$, and $h \approx 0.01$.

[12] The friction factor, f , is sometimes defined as a function of the Reynolds number within the laminar flow regime [Fiedler and Ramirez, 2000]. However, experiments have lead to questions about the applicability of traditional, linear relationships between the Reynolds number and f , finding instead that f may be a non-monotonic function of the Reynolds number [Abrahams et al., 1986; Abrahams and Parsons, 1991]. It has been suggested that the interaction of form roughness, which refers to macroscale bed roughness elements such as gravel or soil clumps, with shallow overland flow may be responsible for the non-monotonic relationships between f and the Reynolds number that have been observed in experiments [Abrahams et al., 1986; Abrahams and Parsons, 1991; Lawrence, 1997]. Additionally, raindrop impact may induce turbulent flow even when the Reynolds number is less than 1000 [Dunne and Dietrich, 1980; Gabet and Dunne, 2003]. Given these complications and the difficulties associated with adequately constraining the additional parameters of a more complex frictional resistance model, f is approximated here as a constant and is determined through comparisons between model predictions and experimental data.

[13] The temporal change in the land surface is defined by

$$\frac{\partial z}{\partial t} = \beta \nabla^2 z + \frac{D - E}{1 - \phi}. \quad (7)$$

[14] The first term on the right-hand side of (7) takes into account the diffusive effect of rain splash with a constant diffusivity, β . The second term represents the fluvial erosion and deposition of sediment. Note that a corresponding diffusive term is not included as a source of sediment within equations (1) and (4). The sediment transported directly through rain splash is never considered to be entrained within overland flow and therefore does not contribute to changes in flow depth or sediment concentration. The fluvial erosion rate, E , is formulated in terms of either stream power, Ω , or shear stress, τ . The stream power erosion law is given by

$$E = \kappa(\Omega - \Omega_c), \quad (8)$$

and the shear stress erosion law by

$$E = \kappa_s(\tau - \tau_c). \quad (9)$$

[15] A critical entrainment threshold, denoted Ω_c for the stream power model and τ_c for the shear stress model, must be exceeded before fluvial erosion occurs. Therefore, $E = 0$ when $\Omega < \Omega_c$ or $\tau < \tau_c$. Additionally, E may be limited by the availability of entrainable sediment, which is described shortly. Here κ and κ_s denote erodibility coefficients for the damaged soil layer and $\Omega = |q||S|$ is the unit stream power with

$$|q| = \sqrt{(uh)^2 + (vh)^2} \quad (10)$$

$$|S| = \sqrt{(\partial z/\partial x)^2 + (\partial z/\partial y)^2}. \quad (11)$$

[16] Shear stress is given by $\tau = h \sin \theta_s$, where θ_s denotes the bed slope. Deposition is computed as $D = cv_s$, where v_s is the particle settling velocity. The depth of the damaged soil layer, v , is initially zero and evolves according to

$$\frac{\partial v}{\partial t} = \zeta A(h, h_c) + \frac{D - E}{1 - \phi} \quad (12)$$

where ζ represents the maximum rate at which the bed is damaged by raindrop impact, h_c is a critical depth of overland flow over which the influence of raindrop impact is assumed to decay, and the function $A(h, h_c)$ modifies the rate at which raindrops damage the original bed material. We assume that the rate at which raindrop impact damages the bed decays exponentially with the ratio of flow depth to the critical depth, h_c , as $A(h, h_c) = \exp(-h/h_c)$. The critical depth, h_c , is likely to scale with characteristic properties of the raindrops such as mean diameter and velocity. In cases where $v > h_c$, it is assumed that the underlying soil is sufficiently shielded so that $A(h, h_c) = 0$.

[17] Through particular choices of the parameters ζ , h_c , and v_s , several different types of erosional environments can be explored. By modeling multiple layers of soil (an erodible and a non-erodible layer), one can study the effects of supply-limited entrainment, where sufficient stream power does not exist to transport the original bed material. We use the term ‘‘supply-limited’’ to distinguish this erosional environment from the traditional detachment-limited model, in which there is no dependence between overland flow depth and the erodibility of the substrate. Also, equation (7) reduces to the usual detachment-limited formulation of sediment transport when $v_s = 0$ and ζ and h_c are sufficiently large so as to not limit sediment entrainment. The addition of an independent deposition rate is useful for simulating erosional environments that exist between the detachment-limited and transport-limited end-member models. A better representation of the total sediment load could be obtained by considering multiple particle size classes, but for this study, a representative particle size is chosen for each simulation. For a given particle size, d , the settling velocity is calculated using the formulation given by Dietrich [1982] for spherical particles.

3.2. Parameter Estimation

[18] Soil bulk densities measured in the Gomez et al. [2003] experiments vary slightly with the surface treatment, but a sediment porosity, $\phi = 0.55$, is chosen to be consistent with the bulk density of the soil, approximately 1200 kg m^{-3} , used within the low-roughness experiments [Gomez et al., 2003]. A value of $h_c = 3 \text{ mm}$, consistent with the diameter of a medium-to-large raindrop, is assumed throughout all numerical simulations. The chosen value of h_c is motivated by experimental results suggesting that the mass of sediment splashed by a raindrop decays exponentially with the ratio of flow depth to raindrop diameter [Dunne et al., 2010]. In the absence of overland flow, the analysis of Dunne et al. [2010] allows for an estimate of $\beta \approx 10^{-9} \text{ m}^2 \text{ s}^{-1}$ when considering an unvegetated surface with a characteristic raindrop diameter of 3 mm , a rainfall rate of 4 cm h^{-1} , and soil bulk density of

approximately 1200 kg m^{-3} . The coefficient of turbulent viscosity is estimated according to $\epsilon = \alpha h \sqrt{ghS}$, where $\alpha \approx 0.2$ [Izumi and Parker, 1995]. Assuming values consistent with typical rill flow within this study, $h = 0.01$ and $S = 0.1$, the coefficient of turbulent viscosity takes a value of $\epsilon \approx 10^{-4}$, which is fixed for the remainder of this analysis.

[19] The rainfall rate and friction factor used within model simulations are chosen to approximately match the discharge and velocity data given by Gomez *et al.* [2003, Figure 13]. Using the Digital Elevation Model (DEM) generated after the second hour of rainfall for both the first and second replications, values of f and R are chosen such that model-predicted discharge rates at the lower boundary of the computational domain are generally on the order of 10^{-2} l s^{-1} with velocities between 0.1 m s^{-1} and 0.3 m s^{-1} within most areas of concentrated flow. This does not uniquely constrain f and R , but the chosen values are consistent with experimental data (Figure 1). When comparing model predictions to experimental data, β is varied within a small range about the estimated value of $\beta \approx 10^{-9}$ given above and the soil erodibility coefficient, κ , maximum rate of soil damage, ζ , particle settling velocity, v_s , and critical entrainment threshold are treated as free parameters.

3.3. Numerical Solution

[20] The numerical solution of the governing equations is simplified slightly by the fact that the landscape evolution equations can be decoupled from the rest of the system. This simplification is justified since erosion occurs on a timescale that is significantly longer than changes in flow depth. Therefore, the general solution strategy is to determine an approximate steady state solution to the overland flow equations and then compute the change in the land surface using the conditions of the steady state flow. This enables more efficient solution of the system over longer total simulation times. The specifics of the numerical method used to solve the overland flow equations are given in detail by Simpson and Castellort [2006] and are only briefly outlined below.

[21] Given an initial topography, a solution to equations (1)–(4) is computed by determining an approximate steady state solution to the time-dependent version of the respective

equations. The criteria used to determine an approximate steady state is the requirement that on average, the percentage change in fluid depth at each node over a 5 s interval is less than 1%. During this phase of each time step, there is no change to the land surface. Once an approximate steady state solution for overland flow is computed, equations (7) and (12) are solved based on the properties of the solution for overland flow and the bed topography is modified. A new steady state flow condition is then found using the modified topography as input, and the process is repeated.

[22] The principal numerical challenge in the model is the integration of the shallow water equations. Average depths of overland flow are generally small and can be less than or on the same order of magnitude as the small perturbations on the land surface. Shock-capturing schemes deal more naturally with the dry/wet interface conditions that can be present in discontinuous shallow overland flow. For this reason, we solve the shallow water equations using a Godunov-type finite volume scheme. Equations (1)–(4) are solved using the HLLC (Harten-Lax-Van Leer-Contact) approximate Riemann solver as described by Simpson and Castellort [2006], with explicit treatment of source terms. The topographic evolution equation (i.e., equation (7)) is then solved using a first-order forward difference in time and a second-order, centered-in-space, discretization of the Laplacian. Equation (12) is also solved with a first-order forward difference in time.

[23] All numerical results are computed on a square grid with a spacing of Δx . Let Q_{ij}^n denote the value of Q at the n th computational time step at a node with x and y positions of $i\Delta x$ and $j\Delta x$, respectively. Defining Δt as the computational time step for the landscape evolution equations, values for z and v at time step $n + 1$ are given by

$$v_{ij}^{n+1} = v_{ij}^n + \Delta t \left(\zeta A(h_{ij}^n, h_c) + \frac{D_{ij}^n - E_{ij}^n}{1 - \phi} \right) \quad (13)$$

$$z_{ij}^{n+1} = z_{ij}^n + \Delta t \left(\beta \frac{z_{i+1,j}^n + z_{i,j+1}^n - 4z_{ij}^n + z_{i-1,j}^n + z_{i,j-1}^n}{\Delta x^2} + \Delta t \left(\frac{D_{ij}^n - E_{ij}^n}{1 - \phi} \right) \right) \quad (14)$$

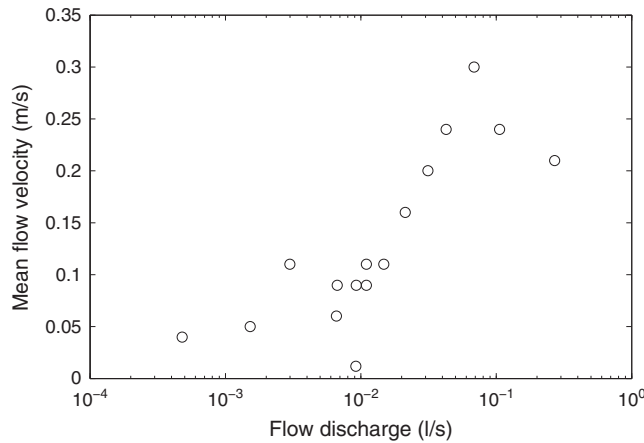


Figure 1. Model-predicted flow discharge versus flow velocity at rill locations corresponding to hour 2 of the Gomez *et al.* [2003] experiments. A DEM corresponding to the experimental surface at $t = 2 \text{ h}$ is used as the input topography to the numerical model. Mean discharge and flow velocity are computed from the model-predicted steady state flow. Values of $f = 0.4$ and $R = 4 \text{ cm h}^{-1}$ are found to be consistent with measurements taken during the experiments [Gomez *et al.*, 2003, Figure 13].

with $E_{i,j}^n$, $D_{i,j}^n$, and $A(h_{i,j}^n, h_c)$ being determined from the steady state values of h , uh , vh , and c . However, while approximating a steady state solution to the overland flow equations, the entrainment rate E is restricted so as to not result in a value of $v < 0$ following the subsequent land-surface update. More specifically, E is restricted so that $E_{i,j}^n \leq \xi(1 - \phi)A(h_{i,j}^n, h_c) + D_{i,j}^n + v_{i,j}^n/\Delta t$. This measure enforces the fact that only material within the damaged layer is capable of being entrained.

[24] Both transmissive and solid boundary conditions are used while computing the solution to equations (1)–(4). If overland flow at a boundary grid point is described by $[h \ uh \ vh \ c]^T = [h_* \ uh_* \ vh_* \ c_*]^T$, then the unknown flow values on the other side of the boundary are specified as $[h \ uh \ vh \ c]_B^T = [h_* \ uh_* \ vh_* \ c_*]^T$ to simulate a transmissive boundary. A solid boundary is simulated by setting $[h \ uh \ vh \ c]_B^T = [h_* - uh_* \ vh_* \ c_*]^T$.

[25] High rates of entrainment and shallow flow on rough topography can occasionally result in isolated pixels with a high sediment concentration. Since this occurs infrequently and the motion of high sediment concentration flows are not adequately modeled by the chosen governing equations, all sediment within the water column in a pixel with $c > 0.2$ is removed from the water column and deposited on the bed.

3.4. Non-Dimensionalization

[26] The landscape evolution equation (i.e., equation (7)) can be simplified in particular circumstances and written in non-dimensional form to elucidate several relevant timescales. In situations where the effects of supply-limited entrainment, deposition of material in suspension, and critical entrainment thresholds can be neglected, the topographic evolution equation can be written in non-dimensional form as

$$\frac{\partial z'}{\partial t'} = \frac{\beta'}{\kappa'} \nabla'^2 z' - |\nabla' z'|, \quad (15)$$

where a prime denotes a dimensionless variable. Here $z' = z/z_0$, $t' = t/t_0$, $\nabla' = L_0 \nabla$, $\beta' = \beta/L_0^2$, $\kappa' = \kappa R_0$, L_0 is the horizontal distance in the along-slope direction, z_0 is the elevation of the hillslope above a base level, R_0 is a characteristic rainfall rate, $R_0 L_0$ is a characteristic discharge, and $t_0 = 1/\kappa'$. One can then see that a timescale associated with rill incision is $t_c = 1/\kappa R_0$ and, more generally, the timescale for the diffusion of a general feature of size λ is $t_d = \lambda^2/\beta$. In this instance, a dimensionless variable, $\theta = \beta'/\kappa'$, similar to a landscape Peclet number can also be defined. Note that θ is the ratio of an advection timescale to a diffusion timescale and can be used as a measure of the relative importance of advective and diffusive sediment transport mechanisms within the system.

[27] In an effort to determine a length scale on which rilling is likely to occur, consider an inclined plane superimposed with low-magnitude roughness elements. Such a surface often develops a parallel drainage network [Simpson and Schlunegger, 2003]. On surfaces with low relative roughness, flow paths are less likely to be diverted from the path of steepest descent and the initial drainage pattern can be expected to consist of parallel flow pathways. Only a portion of the flow pathways suggested by the initial drainage, however, persists long enough to generate rills. Diffusive sediment transport is the mechanism responsible for smoothing incipient rills. Diffusive smoothing

operates more effectively on higher-frequency features, such as those suggested by the initial drainage pattern, but its effectiveness decreases as some micro-rills fail and the lateral frequency of the remaining micro-rills decreases. Eventually, rill incision occurs at a faster timescale than the timescale associated with the diffusion of the developing rills. At this point, developing rills are likely to persist. Although rills may develop at a faster rate at a different lateral frequency, this conceptual model predicts them to develop at the highest frequency at which they are able to form. Namely, in cases where parallel rills form, they are expected to form when $t_d \sim t_c$. Solving for λ yields a length scale for rill spacing,

$$\lambda \sim \left(\frac{\beta}{\kappa R_0} \right)^{1/2}. \quad (16)$$

4. Results

4.1. Comparisons With Experimental Data

[28] In this section, the utility of various subfamilies of the proposed erosion model is tested by comparison with the experimental results of Gomez *et al.* [2003]. The number of rills per cross-slope transect and the mean rill depth were chosen as a means of comparison. In addition to being capable of producing a network with reasonably accurate rill spacing (mean number of rills per transect) and mean rill depth, the success of a particular subfamily of the model was also determined by its ability to predict significant rilling within different portions of the slope at a timescale similar to that observed during the experiments. Rills are identified in the output of the numerical model by scanning along cross-slope transects and tagging pixels with positive curvature above a critical value. Negative values of curvature must then be found within 6 cm of either side of identified points. The average difference between the elevations of the two points of negative curvature and the point of positive curvature must be at least 5 mm in order for the location to be identified as a rill. This identification algorithm leads to a natural means of assigning a depth to each rill location, with the depth being taken as the maximum of the difference between the points of positive and negative curvature. The values of these identification thresholds are likely to vary with the magnitude and frequency of surface roughness elements, but we find that the chosen thresholds correctly identify rill locations for the types of surfaces within this study.

[29] To quantify the ability of the model to accurately predict rill development within different portions of the slope, a technique is used where the slope is partitioned into four different zones. The zones are identified by their fractional distance downslope, ranging from 25 to 100. The portion of the experimental plot consisting of the uppermost 25% of the slope is denoted as fractional distance zone 25, while the lowest 25% of the plot is assigned a fractional distance zone of 100. Rill depth and the number of rills per transect can be averaged within each of the zones to quantify typical values of these variables at different locations on the slope.

[30] For reasons outlined in Gomez *et al.* [2003], the DEMs corresponding to the experimental data do not cover the 0.1 m on either of the lateral sides of the flume or the final 0.4 m of the flume. The computational domain within numerical experiments covers the same region as the DEMs and has a downslope length of approximately 3.6 m and cross-slope length of approximately 1.8 m. A solid boundary is enforced

at the top of the slope, while transmissive boundaries are imposed at both lateral sides and the lower boundary. It is necessary to subsample the pre-rainfall DEM from a resolution of 1.5 mm to 15 mm for computational reasons before it is input into the numerical model. A grid spacing of 1.5 mm severely restricts the time step needed for numerical stability.

[31] In cases where $\xi \gg 1$, $h_c \gg 1$, and $v_s = 0$, the model approximates a detachment-limited erosional environment. It is typical for order of magnitude differences in discharge (and stream power) values to exist between the top and bottom of the slope. Shear stress may similarly vary by several orders of magnitude between areas near the top of the slope, where there is very little flow concentration, and areas at the bottom of the slope. Large spatial variations in stream power and shear stress between the upper and lower portions of the plot are accentuated once channelization begins and encourage scenarios where rills develop and deepen rapidly near the lower boundary and at the same time are unable to form on upper portions of the slope (Figure 2). Numerical results indicate that incision rates within rills significantly increase with time, particularly in the lower portions of the slope (Figure 2), whereas experimental data suggest that rills deepen, on average, at an approximately linear rate after their initial formation (Figures 3a, 3d, and 4b). The shear stress model predicts less rapid growth of rills near the base in comparison to the stream power model but still fails to qualitatively agree with experimental results (Figure 2). A purely detachment-limited erosional environment appears to be insufficient to reasonably describe the development of the experimentally produced rill networks.

[32] Another possibility is to specify $\xi \gg 1$, $h_c \gg 1$, and $v_s > 0$ to account for an erosional environment intermediate to both the detachment-limited and transport-limited extremes. In this manner, the rapid growth of rills at the lower boundary may be impeded by the deposition of sediment as sediment concentrations tend to be highest within the lower portions of the developing rill network. The inclusion of the deposition term reduces overall rill depth, but it appears to be insufficient to significantly alter the large discrepancy between rill growth rates within the upper and lower portions of the plot (Figure 2).

[33] Supply-limited entrainment can be modeled by choosing values of ξ and h_c that are small enough to have a nontrivial effect. Higher water depths shield the underlying bed and decrease the rate at which material becomes available for fluvial detachment and transport. Consequently, entrainment within rapidly developing rills near the boundary tends to be supply limited, while erosion rates in the upper reaches of the network are limited by available stream power (or shear stress). Numerical results obtained in such cases can contain rill networks that evolve, both temporally and spatially, in a manner that is consistent with the results of the *Gomez et al.* [2003] experiments (Figures 3 and 4). Experimental results show rill networks that extend farther up the slope than those suggested by numerical results with the stream power model (Figures 5 and 6). The shear stress model appears to better predicting rill development near the upper boundary of the plot, especially for replication 2 (Figures 5 and 7).

[34] The model, on average, predicts less inter-rill erosion than that observed in experiments. The average amount of total erosion within inter-rill areas in replication 1 of the *Gomez et al.* [2003] experiments is approximately 2 cm, but model-predicted erosion in inter-rill areas is on the order of 0.01 cm and 0.1 cm when using the stream power and shear stress erosion laws,

respectively. Model-predicted overland flow velocities and flow depths tend to be low in these areas, and raindrop impact may exert more control on erosion in such portions of the domain. There is a possible offset zero in the elevation data for replication 2, and therefore, only data from replication 1 are presented. Although this would not influence other computed statistics, such as rill depth or number of rills per cross-slope transect, an offset zero would influence the computed total erosion.

[35] It is found that a spatially and temporally variable erodibility coefficient results in model-predicted rill networks that contain more realistic small-scale sinuosity. In reported results, a mean value of κ is chosen for the entire domain but the value of κ at a particular pixel is drawn from a uniform distribution supported between values that are 30% lower and higher than the mean. The same procedure is applied to κ_s when using the shear stress model, but the distribution of values only varies within a range of 10% around the mean. Temporal changes in substrate erodibility are included by updating κ at a pixel after every 5 mm of incision. Larger variability within the erodibility coefficients results in the development of isolated “holes” within the topography that are not consistent with experiments while significantly less variability in κ or κ_s results in no noticeable change in the rill network.

4.2. Network Geometry

[36] In order to explore controls on rill network geometry and rill spacing, we performed numerical experiments with an initially planar surface superimposed with a given micro-topographic roughness and subjected to steady rainfall. The initial topography is generated by taking the sum of a planar surface with slope S and a random surface, defined by drawing numbers from a normal distribution with zero mean and variance η . The distance between the randomly chosen elevations in both the x and y directions is denoted by δ . In the results discussed below, we use the stream power erosion law and fix the following parameter values: $\Omega_c = 0$, $v_s = 0$, $f = 0.4$, $\xi = 1/90000$, and $h_c = 0.01$. The values for v_s , ξ , and h_c are chosen to approximate a detachment-limited environment, in which the scaling relationships developed earlier are valid.

[37] There are many methods available for characterizing the geometry (e.g., parallel, sub-parallel, dendritic, and sub-dendritic) of large-scale drainage networks. A rill network, consisting of many individual drainages with separate outlets, presents additional difficulties. For instance, a network may contain three rills that reach the end of the slope as first-order channels as well as three rills that are fourth-order channels at the lower hillslope boundary. In such cases, it becomes difficult to assign a single geometry (dendritic or parallel) to the network as a whole. Here, the ratio of rill junctions within the network to the total number of rills, J_r , is taken as a measure of the networks' geometry. Although simple, this method clearly identifies when a rill network consists entirely of parallel channels. The dendritic nature of the network is assumed to increase with J_r . A junction is defined as any pixel that has two distinct rills that drain into it. The mean number of junctions per rill is calculated by first using a steepest descent flow routing algorithm to identify rills as any pixel containing an upstream contributing area greater than a threshold value. However, rills may be more than one pixel in width (cross-slope direction). A thinning algorithm, based on the Rosenfeld-Kak algorithm [*Krishnapuram and Chen*, 1993], is applied to create a rill

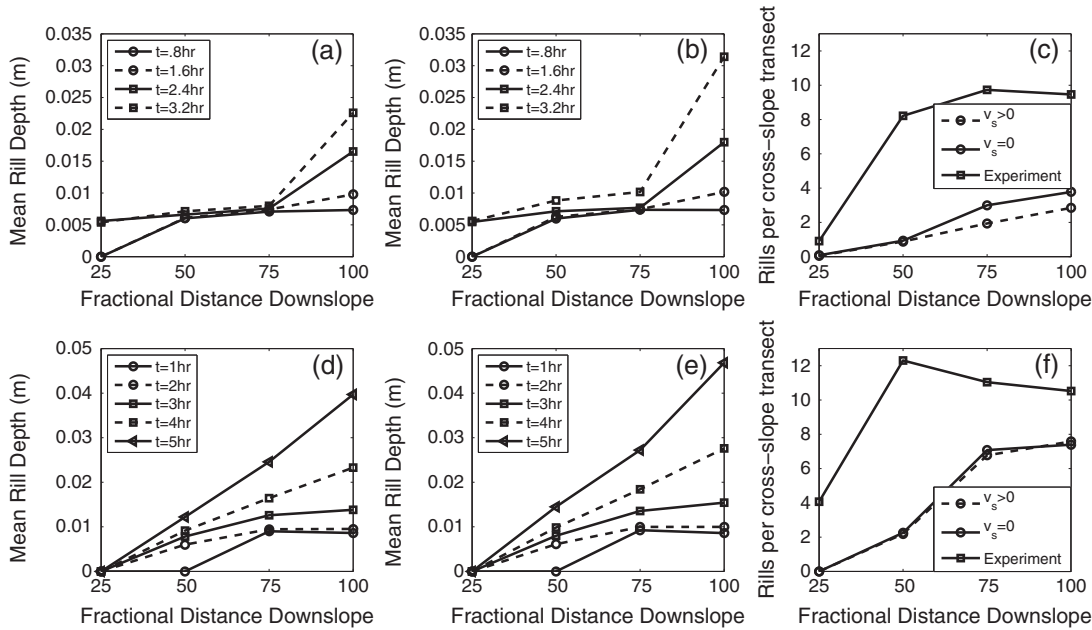


Figure 2. Mean rill depth computed from model-predicted rill networks corresponding to replication 1 of the low-roughness *Gomez et al.* [2003] experiments. (a) Results from using the stream power model with $\zeta = 100$, $h_c = 100$, $v_s = 0.002 \text{ cm s}^{-1}$ ($d \approx 0.006 \text{ mm}$), $\kappa = 0.0175$, and $\beta = 5 \times 10^{-9}$. (b) Results from using the stream power model with $\zeta = 100$, $h_c = 100$, $v_s = 0$, $\kappa = 0.0175$, and $\beta = 5 \times 10^{-9}$. (c) The stream power model ($t = 3.2 \text{ h}$) with $\zeta = 100$ and $h_c = 100$ predicts little rill development in comparison to that seen during the experiments ($t = 3 \text{ h}$). (d) Results from using the shear stress model with $\zeta = 100$, $h_c = 100$, $v_s = 0.002 \text{ cm/s}$, $\kappa_s = 3.5 \times 10^{-3}$, and $\beta = 5 \times 10^{-9}$. (e) Results from using the shear stress model with $\zeta = 100$, $h_c = 100$, $v_s = 0$, $\kappa_s = 3.1 \times 10^{-3}$, and $\beta = 5 \times 10^{-9}$. (f) The shear stress model ($t = 5 \text{ h}$) with $\zeta = 100$ and $h_c = 100$ predicts little rill development in the middle and upper portions of the slope in comparison to that seen during the experiments ($t = 5 \text{ h}$).

map where each rill is a single pixel in width. At this point, junction locations within the network can be determined. This method is used over the previously described rill identification algorithm because it generates a more continuous rill network map, which is necessary for accurate identification of all junctions within the network, rather than one in which a rill may become discontinuous if its depth at a single pixel falls below the 5 mm threshold. Although rill networks within this model are continually evolving in time, we compute final statistics for the networks once the average number of rills per cross-slope transect within the lower third of the slope changes by less than 10% over a time period of 1 h, a timescale comparable to initial rill formation in many cases.

[38] Rills often develop at the lower portions of the slope and extend upslope, deepening with time. Even in the absence of a critical entrainment threshold, the lack of sufficient stream power limits rill formation on the upper portions of the slope (Figures 8–10). Occasionally, rills develop only in the middle portion of the slope, leaving both the upper and lower ends un-dissected. On the lower portion of the slope, the presence of rills can be limited by the supply of entrainable material. At points far enough down the slope, where the flow is sufficiently deep to shield the substrate from raindrop impact, v can be small and the flow is no longer capable of generating incisions within the substrate (Figure 9). Rills then form in an area where flow is sufficiently organized so as to be capable of providing differential erosion but terminate once the flow is deep enough to limit the ability of raindrop impact to aid in the fluvial transport process. In nature, rills that terminate at a given distance downslope

may indicate that typical overland flow events are incapable of transporting material in the absence of other forcing mechanisms (such as rain splash or bioturbation) that act to break down the soil into a more readily transportable state.

[39] Numerical results suggest that both regional slope and surface roughness as well as the ratio of advective to diffusive sediment transport mechanisms are important in determining network geometry (Figures 8, 11, and 12). The drainage pattern suggested by the initial flow pathways is dependent upon the slope and surface roughness, with lower magnitudes of roughness tending to favor initially parallel drainage patterns (Figures 13 and 14). Rill networks developing on such surfaces also tend to be parallel and can consist entirely of first-order channels. When the magnitude of the surface roughness is high, however, initial drainage patterns tend to be more dendritic. In environments dominated by diffusive sediment transport, the final networks are often parallel while they are dendritic, and more similar to the structure of the initial flow pathways, when advective sediment transport is dominant (Figures 13 and 14).

[40] Initial conditions with low-magnitude surface roughness often have initial drainage systems that are parallel (Figure 13). Rill networks that develop and persist on such slopes are also parallel, but with a characteristic spacing that is much greater than that suggested by the initial flow pathways (Figure 10). Numerical results suggest that within the regime of parallel rilling, mean rill spacing tends to occur on a length scale such that the timescale for the diffusion

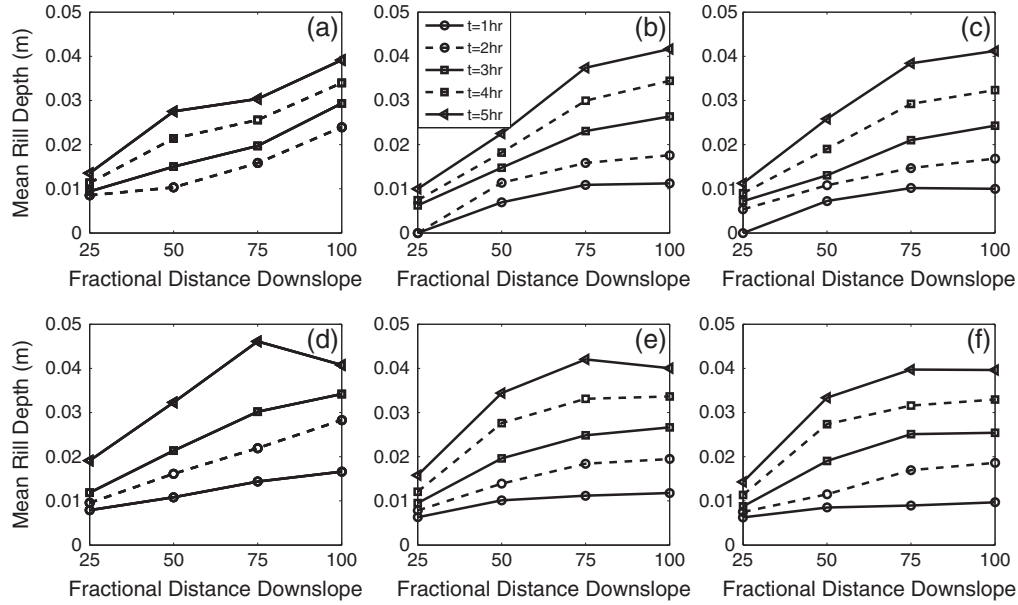


Figure 3. Mean rill depth computed for different portions of the slope. Mean rill depth is computed from DEMs of the *Gomez et al.* [2003] experiments for (a) replication 1 and (d) replication 2. Corresponding numerical model predictions with the stream power erosion law are computed with $\zeta = 1/144000$, $h_c = 0.003$, and $v_s = 0.0002 \text{ cm s}^{-1}$ for (b) replication 1 and (e) replication 2. Corresponding numerical model predictions with the shear stress erosion law are computed with (c) $\zeta = 1/130910$, $h_c = 0.003$, and $v_s = 0$ for replication 1 and (f) $\zeta = 1/120000$, $h_c = 0.003$, and $v_s = 0$ for replication 2. Note that experimental data for hours 1 and 4 are not included from replications 1 and 2, respectively.

of rill-like features is similar to the timescale associated with rill incision (Figures 11 and 12).

5. Discussion

[41] Parallel rills appear to develop on a wider range of initial surfaces than dendritic networks, whose formation requires that roughness elements be preserved for a long enough time to continually divert flow into preferred pathways with a dendritic structure. Even the case of parallel

rilling, sufficient noise is needed to ensure that overland flow concentrates to some degree or the initial surface will erode uniformly. Parallel rills can form on both low and high roughness initial surfaces, but for the idealized surface roughness used in this study, the length scale on which they develop appears to depend mostly on the erosional environment in which they are created.

[42] Often, a large number of periodically spaced flow pathways are present in the initial drainage, but only some fraction of these develops into rills. When initial pathways of overland

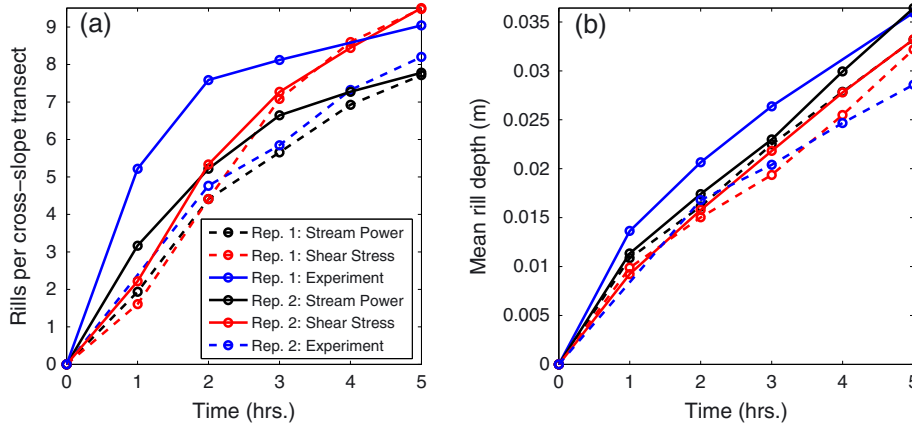


Figure 4. Comparison between model-predicted rill networks and experimental results of *Gomez et al.* [2003] at $t = 5 \text{ h}$. (a) Mean number of rills per cross-slope transect computed from DEMs of experimental results and model predictions with $\zeta = 1/144000$, $h_c = 0.003$, and $v_s = 0.0002 \text{ cm s}^{-1}$. (b) Mean rill depth computed from DEMs of experimental results and model predictions with $\zeta = 1/144000$, $h_c = 0.003$, and $v_s = 0.0002 \text{ cm s}^{-1}$.

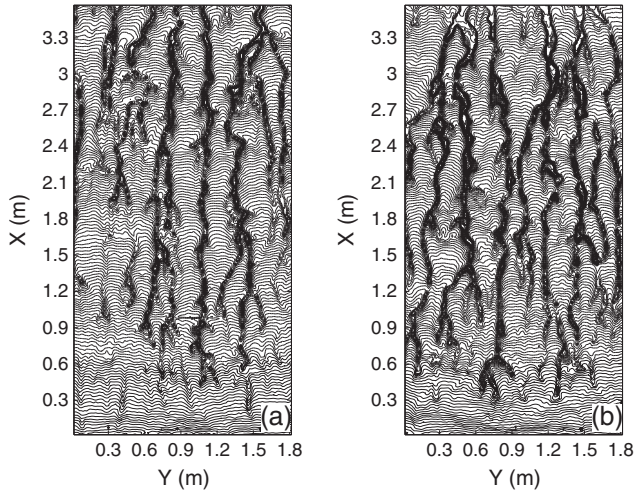


Figure 5. Contour plots of DEMs from experiments of *Gomez et al.* [2003]. (a) Replication 1 at $t=5$ h. (b) Replication 2 at $t=5$ h. Contour intervals are 5 mm.

flow concentration are closely spaced, diffusive transport often dominates any differential fluvial erosion within the resulting tightly spaced erosional features. Less successful micro-rills fail, and the mean spacing between the major flow pathways increases. Remaining micro-rills are less susceptible to diffusive infilling and often inherit a larger percentage of the upstream contributing area. This process continues until fluvial transport dominates diffusive transport within the developing rills. This conceptual model indicates that the spacing of parallel rills is set by the smallest spatial scale for which channel incision occurs faster than the timescale for the diffusive smoothing of rill-like features. Rather than developing at a scale that is optimal, i.e., the scale at which rill-like features may incise the fastest, this suggests that parallel rills form at the smallest spatial scale at which they are capable of being preserved (Figures 11 and 12).

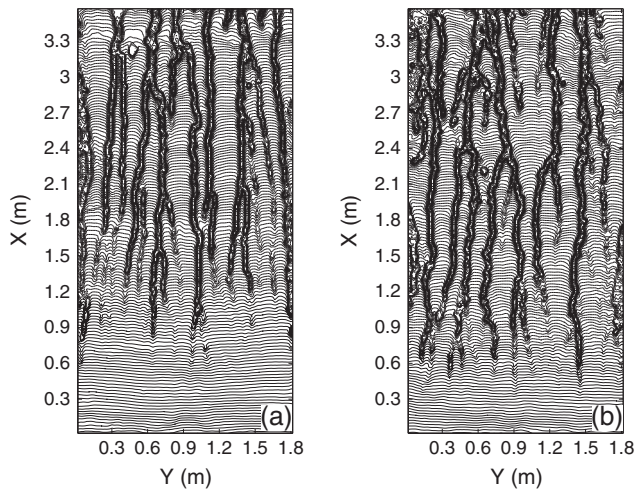


Figure 6. Topographic contours of model-predicted rill networks, using the stream power erosion law, at $t=5$ h. Model predictions corresponding to (a) replication 1 and (b) replication 2 of the experiments performed by *Gomez et al.* [2003]. Contour intervals are 5 mm.

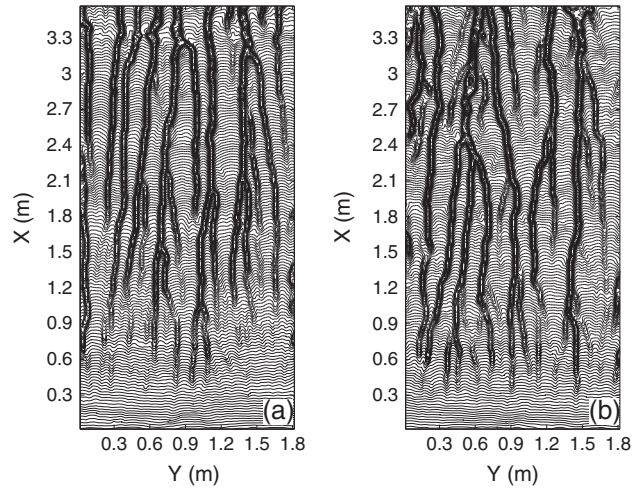


Figure 7. Topographic contours of model-predicted rill networks, using the shear stress erosion law, at $t=5$ h. Model predictions corresponding to (a) replication 1 and (b) replication 2 of the experiments performed by *Gomez et al.* [2003]. Contour intervals are 5 mm.

[43] The applicability of this conceptual model for rill spacing is likely to depend on the properties of the initial surface roughness. If high magnitude, large-scale roughness elements, which are not easily influenced by diffusive sediment transport, continually route flow into the same parallel pathways, the resulting rill spacing may be constant for a wide range of θ values. In general, the proposed scaling relationship is not likely to be applicable in situations where the initial overland flow pathways are widely spaced enough so that the timescale for the diffusion of the developing micro-rills is longer than the timescale for rill incision. Additionally, more complex surfaces may route overland flow more efficiently into fewer pathways, each having relatively high stream power (shear stress), thus requiring smaller values of κ (κ_s), R_0 , and L_0 to accomplish the differential erosion necessary for rill development. In this sense, the rill incision timescale is dependent upon both the statistical properties of the initial surface noise and the regional slope in a manner that is not understood. In numerical simulations, η is chosen to be small relative to the regional slope and we consider only a single frequency of noise, often encouraging flow to initially concentrate on a scale that is sufficiently small such that the timescale for the diffusion of the developing micro-rills is shorter than the timescale for rill incision.

[44] An important relationship between network geometry and the timescale over which the roughness elements diffuse was observed and discussed by *Simpson and Schlunegger* [2003]. Changes between the geometry of the initial flow pathways and the final network can be attributed to the ability, or lack thereof, of the surface roughness elements to repeatedly influence flow patterns. Slopes with large roughness elements have the potential to give rise to dendritic networks, as the roughness elements are more likely to maintain sufficient magnitude so as to preserve initial flow pathways over longer time periods. The roughness elements are capable of repeatedly altering the path of the flow into the same preferred micro-rills and generally only lose this ability once the developing channels are themselves capable of pirating flow. Although dendritic rill networks require

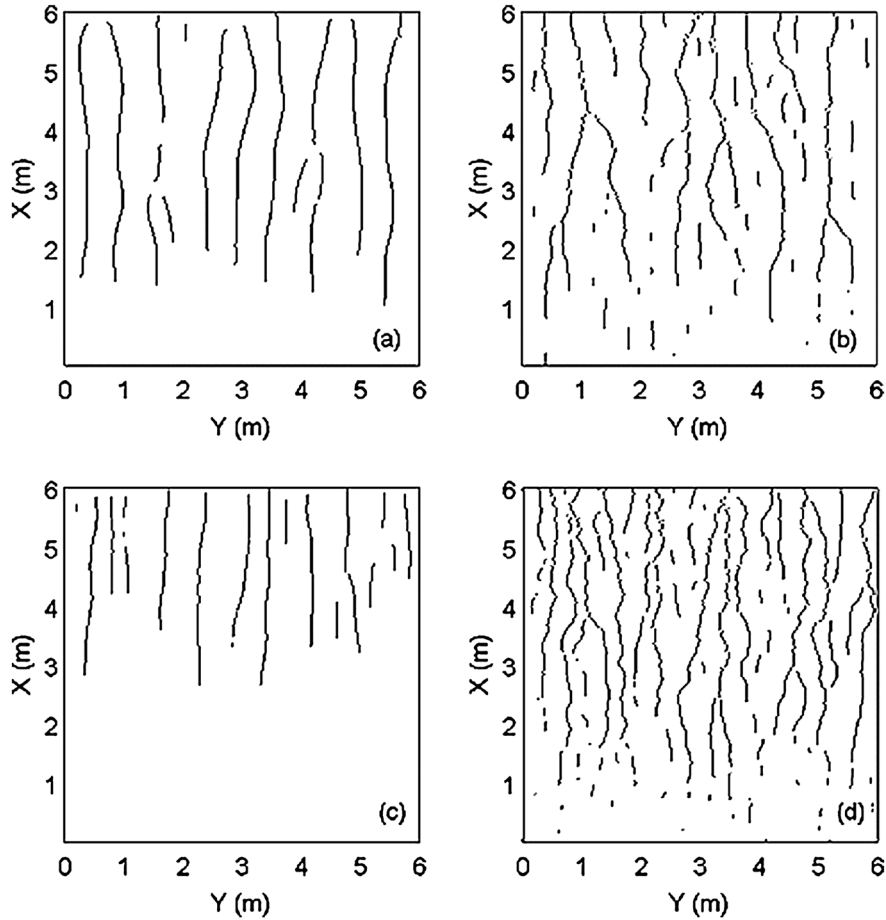


Figure 8. Model-predicted rill networks (black) formed on initially noisy, planar surfaces. Parameter values: $S=0.15$, $\eta=0.03$, and (a) $\delta=0.2$, $\kappa=0.14$, $\beta=10^{-6}$; (b) $\delta=0.2$, $\kappa=0.03$, $\beta=10^{-7}$; (c) $\delta=0.05$, $\kappa=0.03$, $\beta=5 \times 10^{-7}$; and (d) $\delta=0.05$, $\kappa=0.03$, $\beta=10^{-7}$.

surfaces with sufficient noise to generate an initially dendritic drainage pattern, it is common for such surfaces to develop parallel networks due to the dominance of diffusive transport on the scale at which the noise is imposed (Figures 8 and 14b). Such observations suggest that the erosional environment in which the system is formed may

have as significant of an impact on network geometry as the initial topography.

[45] However, critical values of regional slope have been suggested at larger scales that mark transitions between the dominance of parallel and dendritic network types [Castelltort *et al.*, 2009; Jung *et al.*, 2011]. We suggest that in cases where

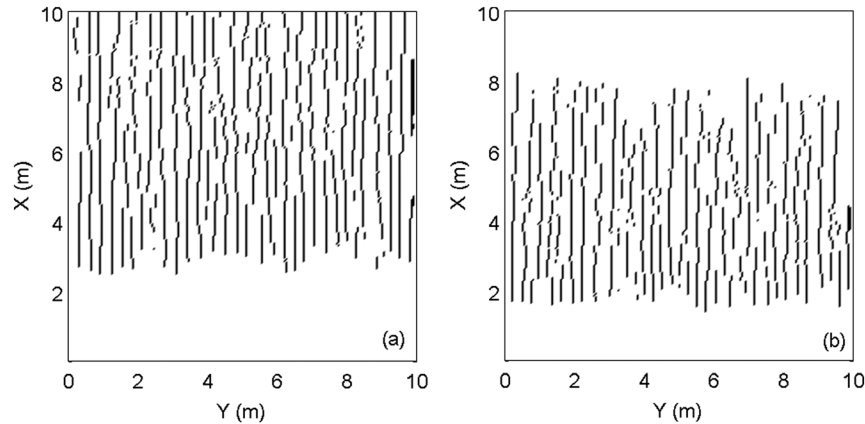


Figure 9. Model-predicted rill networks (black) formed on initially noisy, planar surfaces. Parameter values: $S=0.4$, $\eta=0.001$, $\delta=0.05$, $\kappa=0.09$, $\beta=5 \times 10^{-8}$, $h_c=0.003$, $\zeta=1/120000$, and (a) $R=2 \text{ cm h}^{-1}$; (b) $R=4 \text{ cm h}^{-1}$.

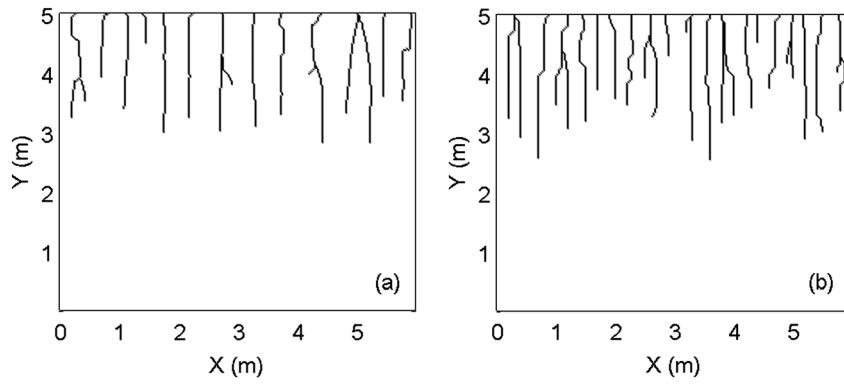


Figure 10. Comparison between initial overland flow pathways and the resulting parallel rill network. (a) Final rill network and (b) major flow pathways on the initial surface.

the initial flow pathways are dendritic, it is possible for the resulting rill network to transition from dendritic to parallel in a gradual manner as the relative importance of diffusive sediment transport is increased (Figure 13). This trend suggests that the transition from dendritic to parallel rill networks is not associated with any particular threshold value. On a larger scale, the typical size of roughness elements and the range of realistic parameter values may not allow for an analogously smooth transition to occur in such instances. In the study of rills, the magnitude of the roughness elements may vary by several orders of magnitude and may be present at such a high frequency that they are extremely susceptible to diffusive smoothing over short timescales, with such changes making them either sufficiently smaller and/or larger than the typical depth of overland flow. One may be able to determine a magnitude of roughness (at a given frequency) that serves as a threshold below which parallel rill networks are favored, but this would likely only include the one class of parallel networks that form from initially parallel drainage patterns and not those which form from initially dendritic patterns.

[46] The landscape evolution equation is the most poorly constrained aspect of this and similar models. The general form of the equations can vary considerably depending on the dominance of particular transport processes. Through particular

choices of the parameters ξ , h_c , and v_s , several different types of erosional environments are represented and two commonly used empirical relationships are used to model fluvial erosion. We find that when comparing numerical results to experimental data, a detachment-limited erosion model leads to the formation of deeply incised rills in the lower portion of the plot with no appreciable rilling on the middle and upper parts of the slope. Including the deposition of sediment within the model has the effect of reducing downcutting in areas with high sediment concentration, which often correspond with rill locations. However, when comparing experimental data with model predictions, including the deposition of suspended sediment does not qualitatively change the results in a significant manner for the cases tested. The idealized erosional environments that did not include rain splash as a limiting factor in fluvial erosion rates were found to be inconsistent with experimental results within all tested portions of the parameter space. The shear stress model performs slightly better than the stream power model in cases where E is not supply limited, but both models fail to be consistent with experimental results. Shear stress and stream power models both compare well with experimental data within supply-limited erosional environments.

[47] Physical systems characterized by high rainfall rates, small spatial scales, and shallow overland flow (such as the

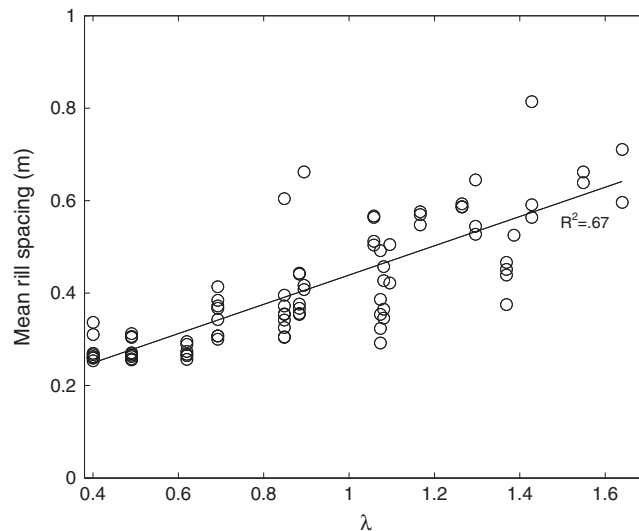


Figure 11. Mean rill spacing as determined from model-predicted networks.

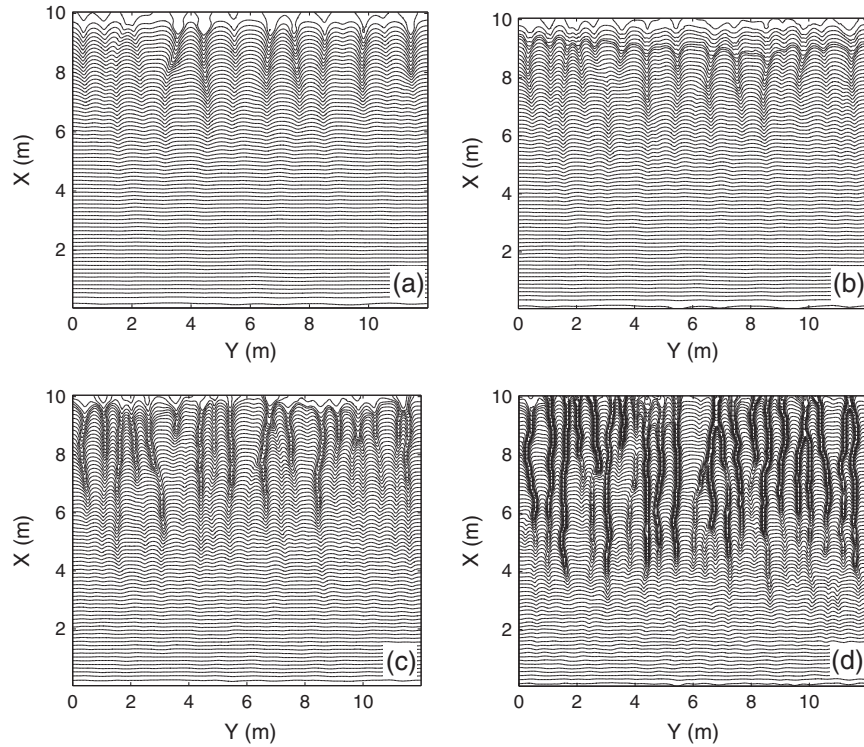


Figure 12. Model-predicted rill networks formed on a rough surface. The initial surface is the same in all cases, but rill spacing decreases as λ decreases. (a) $\lambda = 1.1$. (b) $\lambda = 0.9$. (c) $\lambda = 0.7$. (d) $\lambda = 0.4$. Contour intervals are 1 cm.

Gomez et al. [2003] experiments) are systems in which one might expect raindrop impact to exert control over the fluvial detachment and transport of sediment. High rates of rainfall combined with shallow (or discontinuous) overland flow provide the mechanism through which the soil can be repeatedly impacted by raindrops. Numerical results are consistent with

this hypothesis, demonstrating that such an environment can be adequately modeled within a framework where the only sediment available for fluvial transport lies within a damaged layer of sediment created by the raindrop impact process.

[48] Raindrop impact may have an additional role within the sediment transport process that is not included within

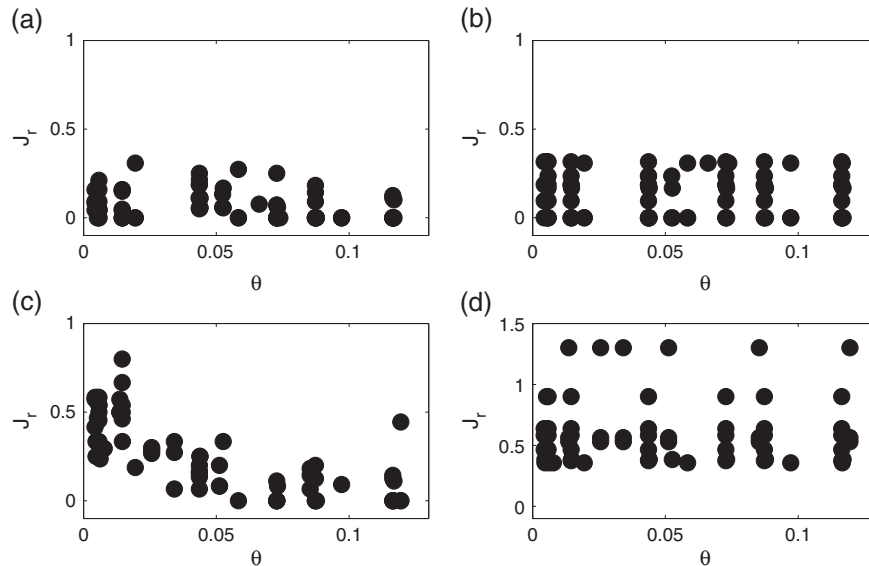


Figure 13. The transition between parallel and dendritic rill networks. (a) J_r calculated from final rill networks formed on planar surfaces with low relative roughness. (b) J_r calculated from the corresponding initial overland flow pathways. (c) J_r calculated from final rill networks formed on planar surfaces with high relative roughness. (d) J_r calculated from the corresponding initial overland flow pathways.

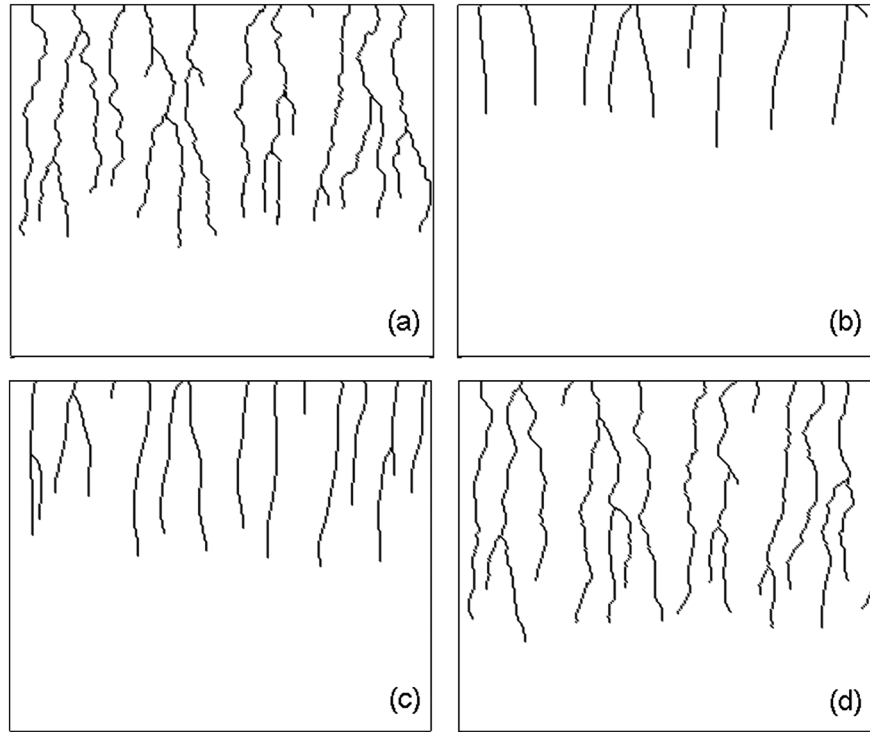


Figure 14. Initial flow pathways and model-predicted rill networks formed on a rough surface. (a) Major flow pathways on the initial surface. Model-predicted rill networks formed on the same initial surface as in (a) when (b) $\theta=0.44$, (c) $\theta=0.22$, and (d) $\theta=0.03$. Model-predicted rill networks transition from parallel to dendritic as θ decreases. When θ is small, the final rill network resembles the initial flow pathways.

the current model. Raindrops can splash sediment into the water column where it may be subsequently transported. The importance of this process is likely to depend on the depth of overland flow, which shelters the underlying sediment from raindrop impact, as well as the distribution of raindrop size and momentum. We expect that including such a process would result in only minor changes within the context of this study by increasing erosion within inter-rill areas. An approximate upper bound on the amount of erosion due to rain splash induced entrainment of sediment can be found by estimating the mass splashed per unit area per unit depth of rainfall, im . Let α_0 and v_t denote the takeoff angle and takeoff velocity of a particle. Based on experiments, *Dunne et al.* [2010] define im for a completely exposed soil surface as

$$im = \frac{2\pi g a r_d^j}{v_t^2 \sqrt{2} \sqrt{1 + 2\cos\alpha_0 \sin\alpha_0}}, \quad (17)$$

where $a=0.0104$, $j=0.927$, and $\alpha_0=11^\circ$ are constants determined from experimental data and r_d is the raindrop diameter. Assuming a drop diameter of 3 mm, and allowing v_t to vary between 1 and 2 m s⁻¹, consistent with reported takeoff velocities for sand particles of varying grain size [*Dunne et al.*, 2010], im can be estimated to be of order 1. With a rainfall rate of 4 cm h⁻¹ and a soil bulk density of 1200 kg m⁻³, this would imply a sediment detachment rate of order 10⁻⁶ m s⁻¹. This is likely an overestimate for several reasons. First, the presence of overland flow will shield the underlying soil. Second, we implicitly assume that all splashed sediment is entrained into the overland flow. In shallow inter-rill areas, τ and Ω are both small and splashed particles may settle back on the bed. Still,

erosion attributed to rain splash induced sediment entrainment may be important for accurately predicting erosion within inter-rill areas, especially over timescales longer than several hours. However, given that erosion due to the direct entrainment of sediment from rain splash is estimated to occur significantly slower than rill incision (approximately 10⁻⁵ m s⁻¹), it is not included in this study.

[49] Sediment entrainment induced by rain splash may be an important process that contributes to the mean lowering of inter-rill areas. A more complex formulation of frictional resistance may also be important in determining erosion rates in shallow inter-rill areas. Typical overland flow depths in inter-rill areas may vary significantly in comparison to the size of surface roughness elements, which may lead to changes in the coefficient of friction in those areas [*Lawrence*, 1997]. The main focus of this study is rill morphology, but including rain splash induced sediment entrainment and a variable friction factor may lead to improved model predictions of inter-rill erosion.

[50] Analysis of the *Gomez et al.* [2003] experiments indicates that rilling occurs at the upper portions of the plot on a timescale that is surprisingly comparable to rill development within the lower portions of the slope despite order of magnitude differences in stream power (and shear stress) within the two regions (Figure 3). Under the assumption that stream power and shear stress are good indicators of the fluvial detachment rate of sediment, it is possible to attribute this effect to a lack of readily transportable material. It is suggested from experiments [e.g., *Gabet and Dunne*, 2003] that the interaction between raindrops and the substrate is responsible for either directly detaching sediment or disturbing the bed in a manner

that makes sediment available for detachment by the flow. When it is assumed that raindrop impact damages a layer of sediment, which can later be more easily eroded, it has the effect of limiting erosion rates at the lower portions of the slope as well as providing a means for material to be more easily transported by the flow in the upslope portions of the plot (Figure 3). The mathematical representation of this process within the model is simplified, and the entrainment of undamaged bed material is not accounted for. It is likely that a second critical threshold exists, particularly for large-scale hillslope erosion problems, after which the flow is capable of transporting undamaged bed material.

[51] One could compute E using friction slope in place of bed slope, which is commonly used in many applications for simplicity. We find that the difference between bed slope and friction slope for a range of rainfall rates and various stages of rill incision is minimal in most areas, with the two slope quantities varying by less than 15% in more than 90% of pixels. Attempting to reproduce experimental results using a model with $\xi \gg 1$ is still not possible with a friction slope formulation of stream power. When using the best fit parameters for replications 1 and 2, the model-predicted mean rill depth and mean number of rills per transect change by less than 15% when using friction slope in place of bed slope.

[52] In the non-dimensionalization of the landscape evolution equation, the erosional environment is assumed to be detachment limited. In numerical results of rill networks on idealized surfaces, the erosional environment only approximates such conditions as v is finite. The values of ξ and h_c were chosen to be small enough to prevent rapid incision of well-developed rills in the lower portions of the slope while still being large enough to avoid the development of terminating rills (Figure 9), an occurrence that might influence mean rill spacing but would not be predicted by the detachment-limited model.

6. Conclusions

[53] A numerical model has been presented for a variably erodible surface subjected to rainfall. The model accounts for three modes of sediment transport: the direct transport of material due to rain splash, the fluvial detachment and transport of bed material damaged by raindrop impact, and the deposition of suspended sediment. It is found that the rate at which original bed material is damaged by raindrop impact may serve as an important mechanism for limiting entrainment rates. Model results agree well with experimental data when raindrop-aided sediment transport is accounted for by allowing the substrate to develop a damaged layer of sediment overlying the undamaged, non-erodible soil. A simplified version of the model using excess stream power or shear stress to determine entrainment rates, without any limitations based on the availability of detachable sediment, is found to be incapable of qualitatively reproducing rill networks formed in physical experiments. Including the deposition of suspended sediment within the model does not have a significant qualitative effect on the ability of the model to match experimental data.

[54] Rill network geometry is found to depend on the relative importance of diffusive and advective sediment transport mechanisms, as quantified by a landscape Peclet number, as well as the initial slope and magnitude of surface roughness. Numerical results suggest that both parallel and dendritic

networks can form on surfaces with high magnitudes of initial roughness while parallel networks dominate over a wide range of parameter values when the magnitude of surface roughness is small. Dendritic networks tend to form when channelization occurs fast enough to develop the micro-rills suggested by the initial flow pattern over a rough surface. Parallel networks generally form when advective transport is small in comparison to diffusive transport or when the initial surface roughness is small. We find no clear critical values of regional slope and/or surface roughness that marks a transition from the prevalence of dendritic to parallel networks. On many of the simple, random surfaces tested, network type can transition from parallel to dendritic as advective sediment transport becomes more dominant than diffusive sediment transport. A scaling relationship for the mean spacing of parallel rills is developed based on a balance between the timescales for the diffusion of rill-like features and fluvial erosion.

References

- Abrahams, A. D., and A. J. Parsons (1991), Resistance to overland flow on desert pavements and its implications for sediment transport modeling, *Water Resour. Res.*, 27(8), 1827–1836.
- Abrahams, A. D., A. J. Parsons, and S. H. Luk (1986), Resistance to overland flow on desert hillslopes, *J. Hydrol.*, 88, 343–362.
- Castellort, S., G. Simpson, and A. Darrioulat (2009), Slope-control on the aspect ratio of river basins, *Terra Nova*, 21(4), 265–270.
- Dietrich, W. E. (1982), Settling velocity of natural particles, *Water Resour. Res.*, 18(6), 1615–1626.
- Dunne, T., and Dietrich, W. E. (1980), Experimental investigation of Horton over-land flow on tropical hillslopes. 2. Hydraulic characteristics and hillslope hydrographs, *Z. Geomorphol. Suppl.*, 35, 60–80.
- Dunne, T., D. V. Malm, and S. M. Mudd (2010), A rain splash transport equation assimilating field and laboratory measurements, *J. Geophys. Res.*, 115, F01001, doi:10.1029/2009JF001302.
- Favis-Mortlock, D. T., J. Boardman, A. J. Parsons, and B. Lascelles (2000), Emergence and erosion: A model for rill initiation and development, *Hydrol. Processes*, 14, 2173–2205.
- Favis-Mortlock, D. (1998), A self-organizing dynamic systems approach to the simulation of rill initiation and development on hillslopes, *Comput. Geosci.*, 24, 353–372.
- Fiedler, F. R., and J. A. Ramirez (2000), A numerical method for simulating discontinuous shallow flow over an infiltrating surface, *Int. J. Numer. Methods Fluids*, 32, 219–240.
- Gabet, E. J., and T. Dunne (2003), Sediment detachment by rain power, *Water Resour. Res.*, 39(1), doi:10.1029/2001WR000656.
- Gilley, J. E., W. J. Elliot, J. M. Laffin, and J. R. Simanton (1993), Critical shear stress and critical flow rates for initiation of rilling, *J. Hydrol.*, 142, 251–271.
- Gomez, J. A., F. Darboux, and M. A. Nearing (2003), Development and evolution of rill networks under simulated rainfall, *Water Resour. Res.*, 39(6), 1148, doi:10.1029/2002WR001437.
- Hairsine, P. B., and C. W. Rose (1991), Rainfall detachment and deposition: Sediment transport in the absence of flow-driven processes, *Soil Sci. Soc. Am. J.*, 55(2), 320–324.
- Hairsine, P. B., and C. W. Rose (1992a), Modeling water erosion due to overland flow using physical principles: 1. Sheet flow, *Water Resour. Res.*, 28(1), 237–243.
- Hairsine, P. B., and C. W. Rose (1992b), Modeling water erosion due to overland flow using physical principles: 2. Rill flow, *Water Resour. Res.*, 28(1), 245–250.
- Heng, B. C. P., G. C. Sander, A. Armstrong, J. N. Quinton, J. H. Chandler, and C. F. Scott (2011), Modeling the dynamics of soil erosion and size-selective sediment transport over nonuniform topography in flume-scale experiments, *Water Resour. Res.*, 47, W02513, doi:10.1029/2010WR009375.
- Izumi, N., and G. Parker (1995), Inception of channelization and drainage basin formation: upstream-driven theory, *Journal of Fluid Mechanics*, 283, 341–363.
- Jung, K., J. D. Niemann, and X. Huang (2011), Under what conditions do parallel river networks occur?, *Geomorphology*, 132, 260–271.
- Kinnell, P. I. A. (1991), The effect of flow depth on sediment transport induced by raindrops impacting shallow flows, *Trans. Am. Soc. Agric. Eng.*, 34(1), 161–168.
- Krishnapuram, R., and L. Chen (1993), Implementation of parallel thinning algorithms using recurrent neural networks, *IEEE Trans. Neural Netw.*, 4(1), 142–147.

- Lawrence, D. S. L. (1997), Macroscale surface roughness and frictional resistance in overland flow, *Earth Surf. Processes Landforms*, 22, 365–382.
- Li, S., and C. J. Duffy (2011), Fully coupled approach to modeling shallow water flow, sediment transport, and bed evolution in rivers, *Water Resour. Res.*, 47, W03508, doi:10.1029/2010WR009751.
- Loewenherz, D. S. (1991), Stability and the initiation of channelized surface drainage: A reassessment of the short wavelength limit, *J. Geophys. Res.*, 96(B5), 8453–8464.
- Nord, G., and M. Esteves (2005), PSEM 2D: A physically based model of erosion processes at the plot scale, *Water Resour. Res.*, 41, W08407, doi:10.1029/2004WR003690.
- Perron, J. T., W. E. Dietrich, and J. W. Kirchner (2008), Controls on the spacing of first-order valleys, *J. Geophys. Res.*, 113, F04016, doi:10.1029/2007JF000977.
- Rieke-Zapp, D. H., and M. A. Nearing (2005), Slope shape effects on erosion: A laboratory study, *Soil Sci. Soc. Am. J.*, 69, 1463–1471.
- Simpson, G., and S. Castellort (2006), Coupled model of surface water flow, sediment transport and morphological evolution, *Comput. Geosci.*, 32, 1600–1614.
- Simpson, G., and F. Schlunegger (2003), Topographic evolution and morphology of surfaces evolving in response to coupled fluvial and hillslope sediment transport, *J. Geophys. Res.*, 108(B6), doi:10.1029/2002JB002162.
- Smith, T. R. (2010), A theory for the emergence of channelized drainage, *J. Geophys. Res.*, 115, F02023, doi:10.1029/2008JF001114.
- Smith, T. R., and F. P. Bretherton (1972), Stability and the conservation of mass in drainage basin evolution, *Water Resour. Res.*, 8(6), 1506–1529.
- Yao, C., T. Lei, W. J. Elliot, D. K. McCool, J. Zhao, and S. Chen (2008), Critical conditions for rill initiation, *Trans. Am. Soc. Agric. Biol. Eng.*, 51(1), 107–114.